Enhanced collisionless shock formation in a magnetized plasma containing a density gradient

S. E. Clark, E. T. Everson, D. B. Schaeffer, A. S. Bondarenko, C. G. Constantin, C. Niemann, and D. Winske

Enhanced collisionless shock formation in a magnetized plasma containing a density gradient

S. E. Clark,[*] E. T. Everson, D. B. Schaeffer, A. S.
Bondarenko, C. G. Constantin, and C. Niemann

Department of Physics and Astronomy,

University of California - Los Angeles, Los Angeles, CA 90095, U.S.A.

D. Winske

Los Alamos National Laboratory, Los Alamos, NM 87545, U.S.A.

Abstract

Two-dimensional hybrid simulations of super-Alfvénic expanding debris plasma interacting with an inhomogeneous ambient plasma are presented. The simulations demonstrate improved collisionless coupling of energy to the ambient ions when encountering a density gradient. Simulations of an expanding cylinder running into a step function gradient are performed and compared to a simple analytical theory. Magnetic flux probe data from a laboratory shock experiment are compared to a simulation with a more realistic debris expansion and ambient ion density. The simulation confirms that a shock is formed and propagates within the high density region of ambient plasma.

---

[*] clarkse@physics.ucla.edu

Collisionless shocks are naturally occurring phenomena which are prevalent in space and astrophysical environments. They occur at the edges of supernova remnants[1], are formed in high altitude ionospheric explosions[2], are formed in front of comets[3], and are formed around Earth as the bow shock[4, 5]. Shocks have been generated in magnetic pinch experiments many years ago[6], though in recent years there has been renewed interest in studying astrophysical-like shocks generated in the laboratory. Currently several different methods are being employed to investigate the formation of shocks, including the collision of two plasma jets[7], and the interaction of two laser-produced plasmas[8]. In these cases the photographic evidence for the formation of a shock and the time scale for formation are suggestive but not conclusive. Novel studies are being carried out with experiments on super-Alfvénic laser-ablated debris expansions in a magnetized background plasma, using the Raptor laser in the Phoenix laser laboratory[9] with the Large Plasma Device (LAPD)[10, 11]. In this paper, we present the first hybrid simulations of shock formation across a density gradient in a parameter regime suitable for laboratory experiments. It is shown that a density gradient aids in coupling energy to the ambient plasma from laser-ablated debris, which improves the effectiveness of the debris piston and generates a stronger shock. Hybrid simulations are then compared to in-situ laboratory data, which support these findings.

Computer simulations with hybrid codes have been used extensively to investigate the coupling physics in the context of high-Mach number plasma interactions[12], astrophysical and high altitude nuclear explosions[13–15], and the structure of collisionless shocks in space[16, 17]. On a much smaller scale, they have also been used to model shock heating[18] and sub-Alfvénic expansions[19] in laboratory experiments, as well as shocks produced by small asteroids in the solar wind.[20]

Previous analytical[21–23] and computational[24, 25] studies on debris-ambient plasma interaction and coupling in our experimental geometry treat the initial ambient plasma as being uniform in density and temperature. These studies typically relate the generation and strength of a shock to a coupling parameter, which was shown to be dependent on the ratio of the equal mass radius ($R_m = R_{b0}\mathcal{M}_A^{-2/3}$) to the directed debris ion gyroradius ($\rho_d = \mathcal{M}_A \frac{m_d/m_i}{Z_d} c/\omega_{pi}$), where $R_{b0} = (\frac{6E_d}{B_0^2})^{1/3}$ is the magnetic stopping radius, E_d is the total debris kinetic energy, B_0 is the background magnetic field, $\mathcal{M}_A$ is the Alfvénic Mach number of the debris expansion, m_d and m_i are the masses of the debris and ambient ion species respectively, Z_d is the charge state of the debris ion species, and c/ω_{pi} is the ambient ion

inertial length[26]. The coupling parameter can also be thought of as a time constraint, or a shock formation time, where $R_m > \mathcal{M}_A v_A t_0$, with $t_0 \sim \frac{\pi}{4}\sqrt{\omega_{ci}\omega_{cd}}$ being the rough shock onset time. The ambient ion inertial length and Alfvénic Mach number of the expansions are inversely proportional to the square root of the ambient ion density, so it becomes a challenge to characterize the coupling parameter using these quantities in the case of an inhomogeneous ambient plasma.

This paper extends previous computational studies to investigate the effects of a density gradient on the coupling of energy from the debris plasma to the ambient plasma. Hybrid simulations are performed in which the debris cloud is treated as a cylindrical expansion passing over a step function density jump. The simulation results are compared to a simple fluid model, initially conceived by Conrad Longmire but rigorously derived by Wright[27], which provides insight into the dependence of the electric and magnetic fields on the ambient ion density. Finally, magnetic flux probe measurements[28] will be compared to a simulation that more closely resembles experimental conditions, in which the debris plasma is modeled as a conical ejection which interacts with a high density core of plasma embedded in a lower density plasma.

The simulation software is a 2D3V collisionless, magnetostatic hybrid code in which there are two Cartesian spatial dimensions, but the fields and velocities are in three dimensions[29]. Two simulations are presented to compare the difference between a cylindrical super-Alfvénic expansion through a uniform background and one with a lower density region near the initial debris cloud. Both simulations have an ambient plasma consisting of H^{+1} with a density $n_i = 10^{13}$ cm^{-3} everywhere, though the nonuniform case has a lower density near the initial debris ions of $n_i = \frac{1}{3} \times 10^{13}$ cm^{-3}, with a radius of 2 c/ω_{pi}. The debris consists of C^{+4} with initial kinetic energy of 50 J, and an expansion velocity of $\mathcal{M}_A \sim 2$. The simulation consisted of 240x240 cells with 100 particles per cell in each species and a grid size of 0.1 c/ω_{pi}. The ambient ion temperature is initialized to $T_i = 1$ eV and the electron temperature to $T_{e0} = 8$ eV. The initial background magnetic field is $B_z = 200$ G, which is perpendicular to the expansion. For the uniform density case, we find that $R_m \sim 5.3$ c/ω_{pi}, $\rho_d \sim 6$ c/ω_{pi}, and the ratio of the two is $R_m/\rho_d \sim 0.9$, where it has been shown that if the coupling parameter is greater than or equal to 0.7 a shock is formed[26]. These parameters are representative of attainable experimental plasma conditions.

Figure 1 displays space-time contour plots of the $\hat{z}$ component of the magnetic field and

the ambient ion density. Figures 1a and 1b are typical of low Mach number shock simulations with a uniform background[26]. Figure 1a shows B_z for the uniform simulation, which indicates a diamagnetic bubble is formed[30], and a compressional electromagnetic pulse separates and propagates away from the edge of the bubble. Fig. 1b displays the ambient ion density being swept out partially in the diamagnetic bubble region. The magnetic field and ambient ion density show compressions on the order of two associated with the wave, which satisfies the Rankine-Hugoniot (RH) jump conditions for a $\mathcal{M}_A \sim 2$ shock[31]. The ion phase space (not shown) indicates that a small percentage of ambient ions are being reflected at the shock front. The combination of the compression satisfying RH jump conditions and the presence of dissipation indicates that the wave can be classified as a shock wave.

The lower panels in Fig. 1 show simulation data from the nonuniform simulation. The results look similar, but there are several noticeable differences. Fig. 1c shows that the shock that is launched is slightly faster than in Fig. 1a. The diamagnetic bubble also extends further spatially. Fig. 1d shows the density compression moving out faster than in the homogeneous case (Fig. 1b), the density is more fully swept out, and the compression is slightly higher.

The results presented in Fig. 1 imply that the coupling of energy and momentum to the ambient ions is stronger in the nonuniform case, resulting in stronger shock generation. This can be understood from the parameter R_m/ρ_d, which has been shown to correlate to the coupling of energy and momentum from debris ions to ambient ions[26]. From simple geometrical considerations, the nonuniform equal mass radius in two dimensions (2D) is $R_{mn}^2 = R_m^2 \times (1 + (1 - \alpha_n)(R_n/R_m)^2)$, where R_n is the radius of the density jump, and α_n is a dimensionless parameter that represents the density fraction in the core ($n_{in} = \alpha_n n_i$). In our case $\alpha_n = 1/3$, which gives a simplified expression: $R_{mn}^2 = R_m^2 \times (1 + 2/3(R_n/R_m)^2)$. So the nonuniform equal mass radius is larger than its uniform counterpart ($R_{mn} > R_m$), which leads to a larger coupling parameter in the nonuniform case ($R_{mn}/\rho_d > R_m/\rho_d$). The nonuniform equal mass radius (R_{mn}) is larger than the uniform case due to the lower density core. This implies stronger coupling for the nonuniform case.

Fig. 2 clearly shows that the coupling of energy and momentum to the ambient plasma is increased in the nonuniform simulation. The ambient ions in the nonuniform simulation start to gain more energy relative to the uniform case around $t\omega_{ci} \sim 0.5$, which is when the pulse is propagating within the low density region. The debris ions in the nonuniform case

4

start to lose a significant amount energy relative to the uniform case around $t\omega_{ci} \sim 1$, when the pulse overruns the density jump.

Since the electric and magnetic fields are responsible for coupling energy and momentum to the ambient ions, one would expect stronger fields in the lower density region, where the coupling is enhanced. Following the procedure outlined in Wright[27], one can derive $\vec{E}$ and $\vec{B}$ for a cylindrical expansion analogously to a spherical expansion. The model assumes unmagnetized debris ions that expand out radially, ambient ions which are stationary and uniform, and completely magnetized electrons that are bound to magnetic field lines. This model neglects electron inertial effects and electron pressure. The magnetic field is modeled as three regions: a cavity where $B_z = 0$, a magnetic field compression in $\hat{z}$ with an associated electric field in $\hat{\phi}$ that causes the electrons to $E_\phi \times B_z$ drift outward radially in a shell, and a region outside of the shell with uniform magnetic field B_0. For a given radius R_s, which is the outside radius of the shell, there is a shell thickness $\Delta R/R_s \approx 1/2 \frac{m_d/m_i}{Z_d} \left(\frac{R_s}{R_m} \right)^2 \propto n_i$ for $(R_s/R_m)^2 \ll 1$. The shell thickness, which is a parameter present in the field solutions, is determined using quasineutrality; thus it is proportional to the ambient ion density. The magnetic field inside the shell can be expressed as $B_z/B_0 = 1 + \frac{Z_d}{m_d/m_i} \left(\frac{R_m}{R_s} \right)^2$, which means that the field compression is inversely proportional to the ambient ion density. The electric field in the shell is given by $E_\phi/B_0 = \mathcal{M}_A \left(\frac{\Omega_i}{\omega_{pi}} \right) \left(\frac{r}{R_s} \right) \frac{Z_d}{m_d/m_i} \left(\frac{R_m}{R_s} \right)^2 \propto n_i^{-3/2}$, where r is the position inside of the shell. These analytical expressions for E_ϕ and B_z dictate that the physical electric and magnetic fields are stronger in lower density background plasmas.

Fig. 3 shows the fields associated with the electromagnetic pulse. While the analytical model and simulation do not match up exactly at early times (not shown) because the initial debris cloud has a finite extent in the hybrid simulation, the simulation shows that the fields are in fact larger as the pulse overruns the density jump at $t\omega_{ci} \sim 1$, which leads to better coupling and energy transfer from the debris ions to the ambient ions. The analytical model is no longer valid after any ambient ions have been swept up, but it does provide some insight into the coupling physics. Launching a magnetosonic pulse into a low density region, which then propagates into a higher density region improves coupling due to larger electromagnetic fields in the compressed electron shell that interact with the ambient ions.

Figure 4 shows several interesting features at a time just before the pulse runs over the density gradient. The azimuthal and radial components of the electric field are larger in the nonuniform (Fig. 4b) simulation at this time compared to the uniform case (Fig. 4a). The

magnetic field compression in the nonuniform case leads the debris ion cloud more than in the uniform case. The phase space (Fig. 4c) shows that the bulk of the ambient ions for the nonuniform case are accelerated to a velocity in excess of twice that of the uniform case. The stronger E_ϕ accelerates the ambient ions faster in the nonuniform case, which then turn upstream in the enhanced magnetic field and get ahead of the piston[15]. The density is swept out more effectively behind the magnetic pulse due to the larger electric field, as shown in Fig. 4d. In the low density region of the nonuniform simulation a larger percentage of debris ions participate in transferring energy to the ambient ions and do not slip out past the cavity, or do not "decouple" in the parlance of Hewett[15]. The enhanced coupling in the low density region limits the number of particles that "decouple," which increases the energy transferred to the ambient ions.

These hybrid simulations have been validated by laboratory experiments in the LAPD. The latest LAPD experiment[32] utilized a recent upgrade which consists of a lanthanum-hexaboride (LaB_6) cathode[33] at the North end of the machine to compliment the original barium-oxide (BaO) coated Nickel cathode at the south end of the machine. The combination of these two cathodes, with different electron emissivity, yields a radially inhomogeneous ambient plasma. The ambient plasma consists of singly ionized hydrogen (H^{+1}) ions with a peak density in the center of the machine of $n_i \sim 1 - 2 \times 10^{13}$ cm^{-3} and a diameter of 20-40 cm. This high density plasma is embedded in a larger diameter plasma of ~ 80 cm that has a density $n_i \sim 2 \times 10^{12}$ cm^{-3}. The target used in the experiment consisted of high density polyethylene which was positioned just outside of the high density region, 30 cm off axis. The laser blow-off plasma then passes through a density gradient during the initial expansion phase from a low density region into a higher density region. The measured density profile peaked at 2.2×10^{13} cm^{-3} at a distance of 30 cm. The shape is roughly Gaussian, with a standard deviation of $\sigma \sim 18$ cm. The density was $n_i \sim 2 \times 10^{12}$ cm^{-3} outside of the high density region. This ambient density profile is used in the hybrid simulation. The background magnetic field is 400 G.

Fig. 5 shows the measured B_z in the experiment, which compares well with the simulation. The simulation was performed using 240x240 cells with 100 particles per cell, in a domain that extends to 32 c/ω_{pi} in X and Y, where the ion inertial length is defined by the peak density. The debris ions were initialized such that the radial velocity spread is on the order of the drift velocity, which is $\mathcal{M}_A \sim 1.5$, consistent with spectroscopic Doppler shift

measurements. They are ejected out conically at $\pm 30°$ off of the x-axis. The electrons have reference temperature $T_{e0} \sim 6$ eV, and the ambient ion temperature is 1 eV, which corresponds with measured values of temperature calculated from Langmuir probes. Fig. 5a shows a compression that is broadening and separating from the piston in the high density region. The ramp up at the front of the wave and the compression ratio are in line with RH jump conditions for a Alfvénic Mach 2 shock. The compression decreases after propagating into the lower density region at around 40 cm from the target. The simulation depicted in Fig. 5b shows average compressions around the same magnitude. The ambient ion phase space in the simulation (not shown) shows the presence of reflected ions, which indicates that the magnetosonic pulse in the experiment has in fact steepened into a sub-critical shock.

In summary, this paper takes a first look at extending shock formation theory to more realistic conditions with the aid of hybrid simulations that have been benchmarked by experimental data. In contrast, previous theories for shock formation using diamagnetic bubbles as a piston typically consider the ambient ions as initially uniform, and the expansion as either cylindrically or spherically symmetric. It has been shown analytically and computationally that a density gradient enhances coupling, reduces the shock formation time and increases the Mach number of the shock, which are important for the design of laboratory shock experiments.

[1] D. S. Spicer, R. W. Clark, and S. P. Maran, Astrophys. J. **356**, 549 (1990).

[2] P. Dyal, J. Geophys. Res. **111**, A12211 (2006).

[3] N. Omidi and D. Winske, J. Geophys. Res. **92**, 13,409 (1987).

[4] C. T. Russell and E. W. Greenstadt, Space Science Reviews **23**, 3 (1979).

[5] C. P. Escoubet, M. Fehringer, and M. Goldstein, Annales Geophysicae **19**, 1197 (2001).

[6] M. Keilhacker, M. Kornherr, and K.-H. Steuer, Z. Physik **223**, 385 (1969).

[7] E. C. Merritt, A. L. Moser, S. C. Hsu, C. S. Adams, J. P. Dunn, A. M. Holgado, and M. A. Gilmore, Phys. Plasmas **21**, 055703 (2014).

[8] H.-S. Park, D. D. Ryutov, J. S. Ross, N. L. Kugland, S. H. Glenzer, C. Plechaty, S. M. Pollaine, B. A. Remington, A. Spitkovsky, L. Gargate, et al., High Energy Density Physics **8**, 38 (2012).

[9] C. Niemann, C. G. Constantin, D. B. Schaeffer, A. Tauschwitz, T. Weiland, Z. Lucky, W. Gekelman, E. T. Everson, and D. Winske, Journal of Instrumentation **7**, P03010 (2012).

[10] W. Gekelman, H. Pfister, Z. Lucky, J. Bamber, D. Leneman, and J. Maggs, Rev. Sci. Instrum. **62**, 2875 (1991).

[11] C. Niemann, W. Gekelman, C. G. Constantin, E. T. Everson, D. B. Schaeffer, S. E. Clark, D. Winske, A. B. Zylstra, P. Probyl, S. K. P. Tripathi, et al., Phys. Plasmas **20**, 012108 (2013).

[12] V. A. Thomas and S. H. Brecht, Phys. Fluids **29**, 2444 (1986).

[13] D. Winske and S. Gary, J. Geophys. Res. **112**, A10303 (2007).

[14] S. H. Brecht, D. W. Hewett, and D. J. Larson, Geophys. Res. Lett. **36**, 15 (2009).

[15] D. W. Hewett, S. H. Brecht, and D. J. Larson, J. Geophys. Res. **116**, A11310 (2011).

[16] M. M. Leroy, D. Winske, C. C. Goodrich, C. S. Wu, and K. Papadopoulos, J. Geophys. Res. **87**, 5081 (1982).

[17] B. Lembege, J. Giacalone, M. Scholer, T. Hada, M. Hoshino, V. Krasnoselskikh, H. Kucharek, P. Savioni, and T. Terasawa, Space Sci. Rev. **110**, 161 (2004).

[18] A. G. Sgro and C. W. Nielson, Phys. Fluids **19**, 126 (1976).

[19] N. T. Gladd and S. H. Brecht, IEEE Trans. Plasma Sci. **20**, 678 (1992).

[20] X. Blanco-Cano, N. Omidi, and C. T. Russell, J. Geophys. Res. **108**, 1216 (2003).

[21] R. P. Drake, Phys. Plasmas **7**, 4690 (2000).

[22] Y. P. Zakharov, IEEE Trans. Plasma Sci. **31**, 1243 (2003).

[23] C. Constantin, W. Gekelman, P. Pribyl, E. Everson, D. Schaeffer, N. Kugland, R. Presura, S. Neff, C. Plechaty, S. Vincena, et al., Astrophys. Space Sci. **322**, 155 (2009).

[24] A. I. Golubev, A. A. Solov'ev, and V. A. Terekhin, J. Appl. Mech. Tech. Phys. **19**, 602 (1979).

[25] V. P. Bashurin, A. I. Golubev, and V. A. Terekhin, J. Appl. Mech. Tech. Phys. **24**, 614 (1983).

[26] S. E. Clark, D. Winske, D. B. Schaeffer, E. T. Everson, A. S. Bondarenko, C. G. Constantin, and C. Niemann, Phys. Plasmas **20**, 082129 (2013).

[27] T. P. Wright, Phys. Fluids **14**, 1905 (1971).

[28] E. T. Everson et al., Rev. Sci. Instrum. **80**, 113505 (2009).

[29] D. Winske and K. B. Quest, J. Geophys. Res. **93**, 9681 (1988).

[30] D. B. Schaeffer, E. T. Everson, D. Winske, C. G. Constantin, A. S. Bondarenko, L. A. Morton, K. A. Flippo, D. S. Montgomery, S. A. Gaillard, and C. Niemann, Phys. Plasmas **19**, 070702 (2012).

[31] R. A. Treumann, Astron. Astrophys. Rev. **17**, 409 (2009).

[32] D. B. Schaeffer, E. T. Everson, A. S. Bondarenko, S. E. Clark, C. G. Constantin, S. Vincena, B. V. Compernolle, S. K. P. Tripathi, D. Winske, W. Gekelman, et al., Phys. Plasmas **21**, 056312 (2014).

[33] C. M. Cooper, W. Gekelman, P. Pribyl, and Z. Lucky, Rev. Sci. Instr. **81**, 083503 (2010).
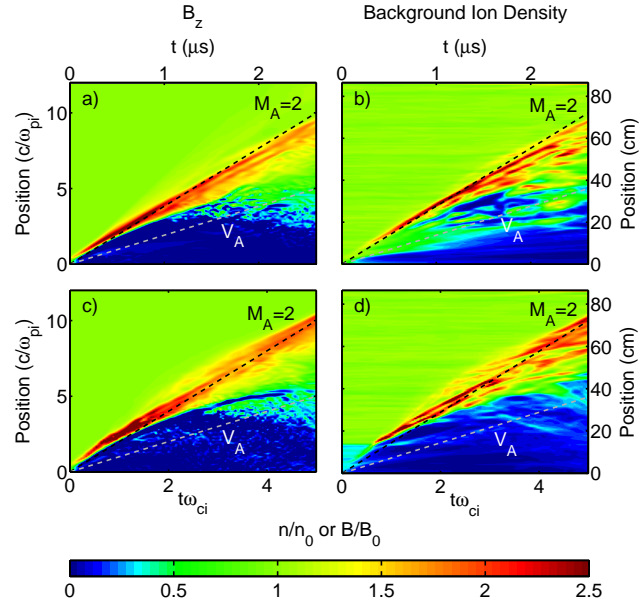
FIGURES

9

(Color online) Space-time contour plots for two comparative hybrid simulations. The first row shows (a) B_z and (b) ambient ion density for the simulation case with uniform initial background density. Panels (c) and (d) show the same plots, but for the case with nonuniform ambient ion density. Each panel shows spatial profiles along a line through the domain for $x > 0$ and $y = 0$, as a function of time.

Ion Kinetic Energy

- - - Uniform – Debris Ions
- - - Non Uniform – Debris Ions
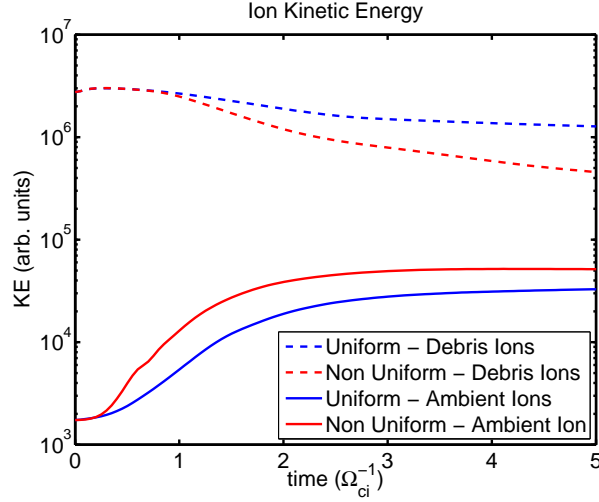—— Uniform – Ambient Ions
—— Non Uniform – Ambient Ion

FIG. 2: (Color online) Kinetic energy of ambient ions (solid) and debris ions (dashed) for the uniform (blue/outer) versus the nonuniform (red/inner) simulation calculated from a sampling of particle data, which shows improved energy coupling to the ambient ions in the nonuniform case.
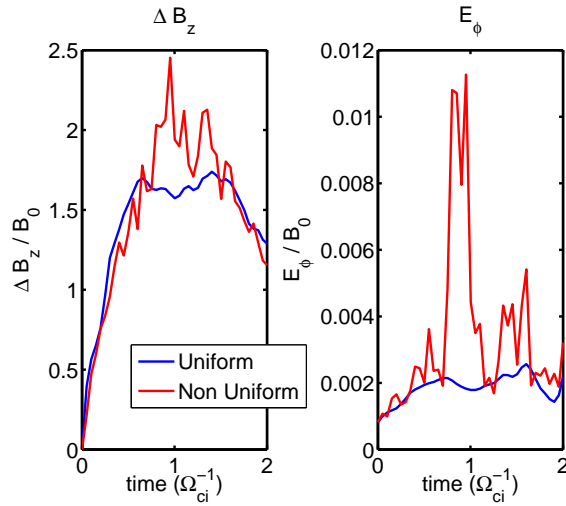

ΔB_z

E_ϕ

—— Uniform
—— Non Uniform

FIG. 3: (Color online) $\Delta B_z/B_0$ and E_ϕ/B_0 maximum values on the line $x > 0$ and $y = 0$ vs. time for uniform (blue/lower line) and nonuniform (red/upper line) simulations.
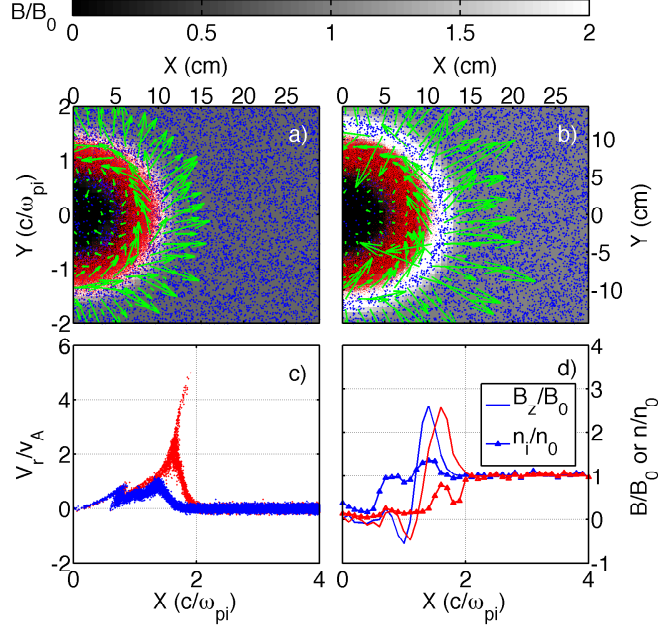
10

FIG. 4: (Color online) Simulation output at a time $t\omega_{ci} \sim 0.5$. Panels (a) and (b) are composite figures which show B_z in grayscale over the simulation domain, a sampling of debris ions (red) and ambient ions (blue), as well as relative electric field strength and direction (green arrows). Panel (c) shows an overlay of the phase space of the ambient ions for the uniform (blue/lower) and nonuniform (red/upper) simulations. Panel (d) shows overlays of the magnetic field for uniform (blue line to left) and nonuniform (red line to right) cases as well as ambient ion density for the uniform (blue/upper line with triangles) and nonuniform (red/lower line with triangles) simulations.
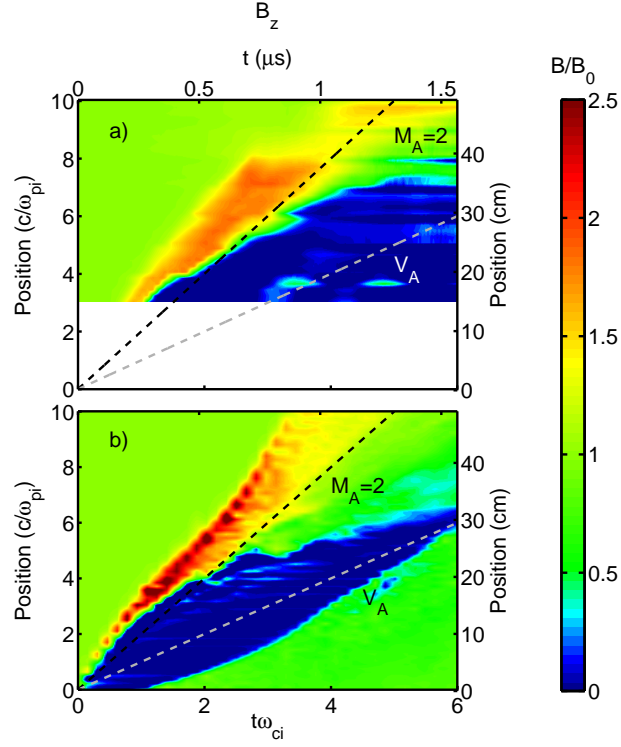
FIG. 5: (Color online) (a) Experimental magnetic flux probe data collected over a series of laser shots compared to (b) B_z output from a simulation with plasma parameters comparable to the experiment from a line through the domain for $x > 0$ and $y = 0$.